Design of a radio frequency quadrupole for a high intensity heavy-ion accelerator facility

Zhouli Zhang,[1,2] Xianbo Xu,[1] Yuan He,[1] Shengxue Zhang,[1] Chao Wang,[1,2] Shenghu Zhang,[1] Chenxing Li,[1,*] and Yulu Huang[1,†]

[1]*Institute of Modern Physics, Chinese Academy of Sciences, Lanzhou 730000, People's Republic of China*
[2]*School of Nuclear Science and Technology, University of Chinese Academy of Sciences, Beijing 100049, People's Republic of China*

(Received 7 September 2021; revised 13 June 2022; accepted 11 July 2022; published 8 August 2022)

We report a design work of a continuous-wave (cw) radio frequency quadrupole (RFQ) for the injector linac of the High Intensity heavy-ion Accelerator Facility project. The rf design and multiphysics analysis were conducted to enhance the long-term stability and reliability of the cavity. To minimize the peak modified Poynting vector and peak surface electric field associated with the rf breakdown rate, the cross section and the vanes segmentation of the RFQ cavity were optimized. Pi-mode stabilizing loops (PISLs) were adopted for the cavity to increase the mode separation between the quadrupole and the neighboring dipole modes, intending to reduce the emittance growth and beam loss caused by the field asymmetry of the quadrupole mode. Due to the lack of a universal criterion of acceptable mode separation, the field asymmetry of the quadrupole mode was directly used as the design criterion for the PISL. Tuners were designed to tune the cavity frequency and longitudinal field flatness. Thermal distributions on tuners with and without rf sealing were investigated, and we found that rf sealing was indispensable in decreasing the tuner's temperature. A multiphysics analysis was carried out to maintain the cavity frequency while running with different rf power, in an attempt to avoid frequently adjusting the cooling water temperature when accelerating different ions. The analysis also verified that a large wall thickness could make the cavity possess a low stress and a minor deformation.

DOI: 10.1103/PhysRevAccelBeams.25.080102

I. INTRODUCTION

The High Intensity Heavy-Ion Accelerator Facility (HIAF) project at the Institute of Modern Physics (IMP), Chinese Academy of Sciences is characterized by unprecedented heavy ion beam intensities (e.g., 1×10^{11} ppp for $^{238}U^{35+}$ in the Booster Ring) and hence gives scientists great opportunity to explore the hitherto unknown territories in the nuclear chart and to open new domains of physics researches in experiments [1]. To produce the intense stable and radioactive beams with ions energies ranging from MeV/u to GeV/u, the scheme of coupling superconducting linear accelerator with high-energy synchrotrons was selected [see Fig. 1(a)]. Highly charged ion beams are generated by the superconducting electron-cyclotron-resonance ion source (SECR) and then are accelerated by the ion linear accelerator [iLinac, see Fig. 1(b)], which consists of a room-temperature radio frequency quadrupole (RFQ) of 81.25 MHz, 30 QWR (quarter-wave resonator) superconducting cavities with the same frequency and 66 HWR (half-wave resonator) superconducting cavities of 162.5 MHz, to the energy of 17 MeV/u with a charge-to-mass ratio of 1/7. Next, the ion beams are injected into the Booster Ring (BRing) to reach the intensity of 1×10^{11} ppp and then accelerated further to the energy of 800 MeV/u for $^{238}U^{35+}$. Finally, the beams are extracted either to the external targets or transferred to the Spectrometer Ring (SRing) for a variety of experiments. Additionally, some experimental setups will also be built at the end of the iLinac.

As an intense and high-power user facility, long-term stability and reliability are the primary concerns for the HIAF project. The low energy section, consisting of a low energy beam transfer line and an RFQ, affects the stability and reliability a lot due to the strong space charge effects. In particular, the RFQ is one of the main unstable sources in which the rf electric breakdown, the thermal problems, and the crack of coupler vacuum windows often happen [2–4].

*Corresponding author.
lichenxing@impcas.ac.cn
†Corresponding author.
huangyulu@impcas.ac.cn

Published by the American Physical Society under the terms of the Creative Commons Attribution 4.0 International license. Further distribution of this work must maintain attribution to the author(s) and the published article's title, journal citation, and DOI.

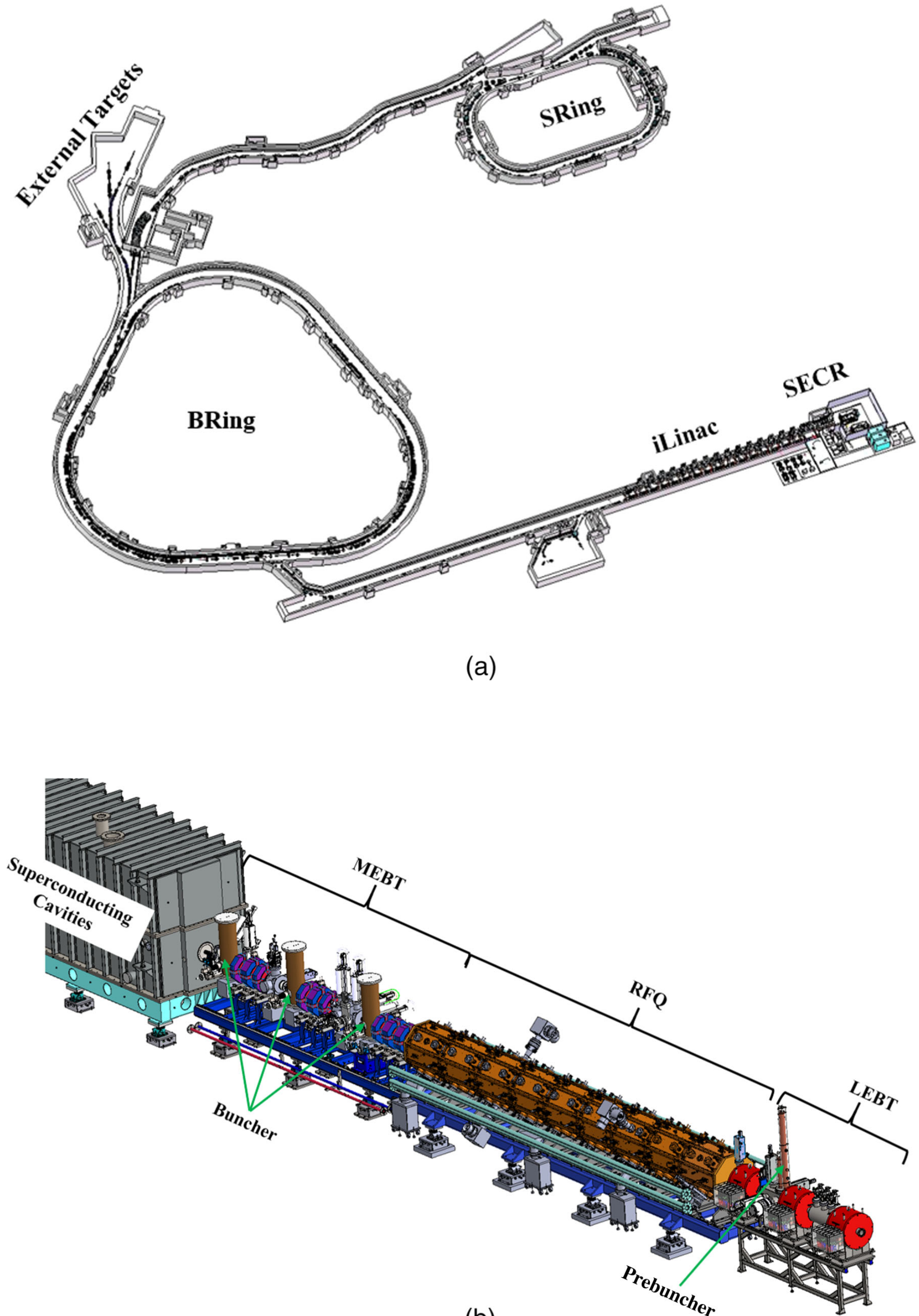

FIG. 1. (a) Layout of the HIAF project; (b) Layout of the HIAF injector linac (iLinac).

Therefore, to improve the stability and reliability of the RFQ, the peak surface electric field, mode separation, tuner design, and layout of cooling water channels were investigated and optimized during the cavity design.

This paper describes the design of the HIAF RFQ and is organized as follows: First, the beam dynamics design of the HIAF RFQ is introduced; second, rf design of the RFQ cavity is presented, which focuses on the reduction of peak modified Poynting vector and peak surface electric field, and the method to improve the field symmetry; third, a multiphysics analysis of the cavity is shown; finally, a summary is given.

TABLE I. Main beam dynamics parameters of HIAF RFQ.

Parameter	Value
Designed particle	$^{238}U^{35+}$
Frequency [MHz]	81.25
Input/output energy [MeV/u]	0.014/0.8
Intervane voltage [kV]	75
Current [mA]	2
Maximum surface field [MV/m]	18.09
Average aperture r_0 [mm]	5.81
Radius of curvature of vanes ρ [mm]	4.36
Vane length [mm]	8549.86
Transmission efficiency [%]	99.8

II. BEAM DYNAMICS DESIGN OF THE HIAF RFQ

Working at the frequency of 81.25 MHz, the HIAF RFQ aims at accelerating particles with a charge-to-mass ratio of up to 1/7, increasing the energy of the particles from 0.014 MeV/u to 0.8 MeV/u in a length of 8.55 m. Depending on the particle type, the RFQ was designed to work in cw or pulse mode, and the KP factor (also known as "bravery factor" [5]) was controlled below 1.6 and 2.0 for the two modes to reduce the rf breakdown rate. Beam intensity varies for different particles, for instance, 2 emA for $^{238}U^{35+}$, 0.5 emA for $^{238}U^{46+}$, and 0.6 emA for H_2^+. An external three-harmonic prebuncher will be placed before the RFQ to reduce the output longitudinal emittance and shorten the cavity length. The main beam dynamics parameters of the RFQ are listed in Table I.

III. RF DESIGN OF THE HIAF RFQ

Due to the low power consumption density and simple cooling channel layout, the four-vane structure (as shown in Fig. 2) was adopted for the HIAF RFQ to deal with the thermal problem effectively when working in cw mode. To reduce the potential impact of the dipole modes on the operating quadrupole mode [6], we chose the pi-mode stabilizing loops (PISL [7], as shown in Fig. 2) to achieve the goal. This section mainly focuses on the approaches to improve the cavity's stability and reliability, including optimization of the cross section, the PISL, the tuners, the vanes segmentation, and the undercut. The simulation of the whole cavity is presented as well.

A. Cross-section optimization

The cross section of the HIAF RFQ is shown in Fig. 3, where the parameters r_0 and ρ are given by the beam dynamics design and the other nine parameters are to be optimized. The main goal of the cross-section optimization is to minimize the peak modified Poynting vector (Sc_peak) [8]. The quantity Sc_peak is related to the rf breakdown rate, the probability of a breakdown during an rf pulse. It is derived from an rf breakdown trigger model, in which field emission currents from potential breakdown sites lead to local pulsed heating. It is proportional to the product of the electric field and magnetic field and has been used to guide the design of high-gradient accelerating structures with frequencies around 3 GHz or higher [9,10]. Despite the good separation of the electric and magnetic fields in an RFQ [11], the small amount of magnetic field in the vane-tip region, where the electric field dominates and rf breakdown usually happens, would enhance the rf breakdown. Therefore, it is essential to investigate the modified Poynting vector in the vane-tip region.

The cross-section optimization was conducted with a slice of 1 mm in thickness. The optimization results show

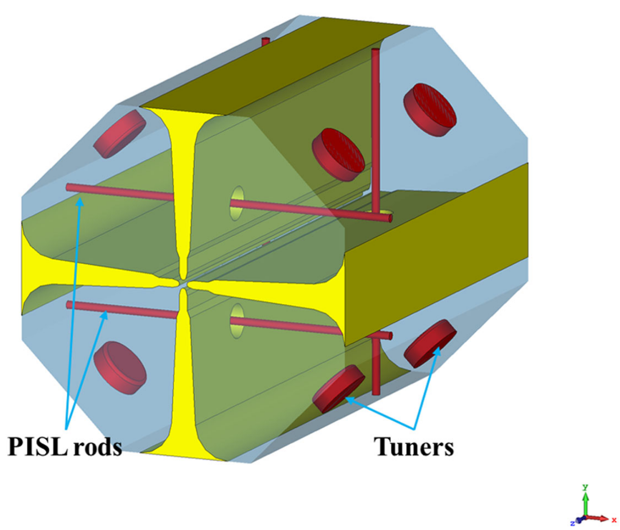

FIG. 2. Four-vane RFQ structure.

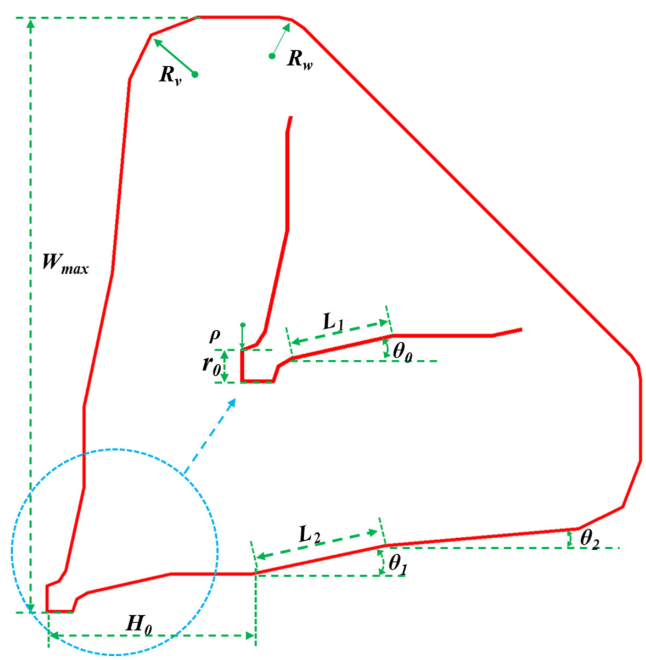

FIG. 3. Cross section of the HIAF RFQ.

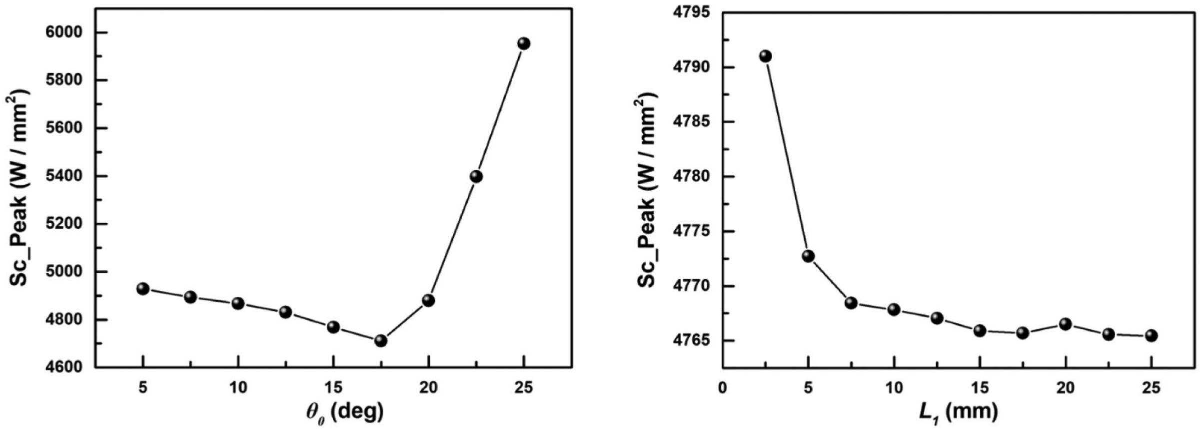

FIG. 4. Influences of θ_0 and L_1 on Sc_peak.

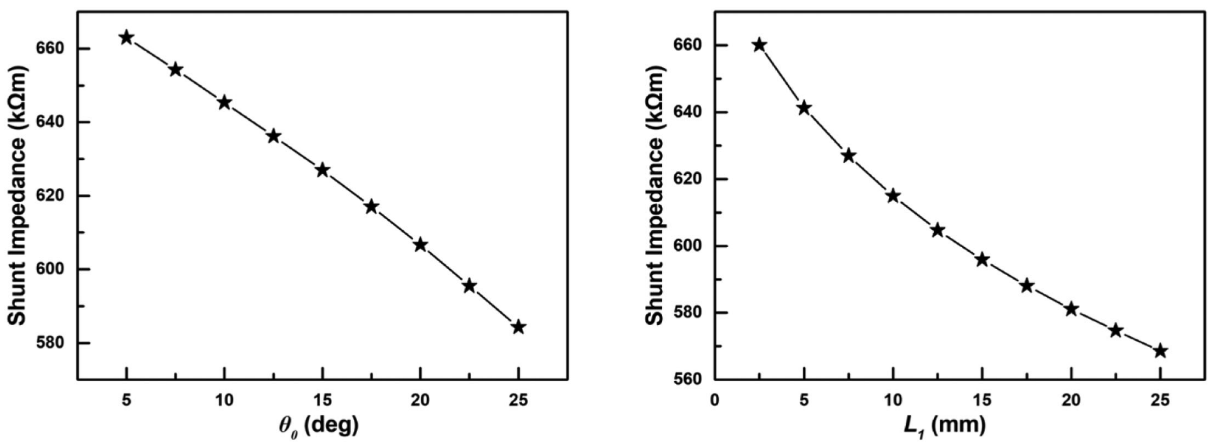

FIG. 5. Influences of θ_0 and L_1 on shunt impedance.

that there exists an optimal breakout angle θ_0 with a minimum Sc_peak, and a large L_1 is pursued to get a low Sc_peak (see Fig. 4). However, the shunt impedance of the cavity decreases fast with increasing θ_0 and L_1, as shown in Fig. 5. Finally, θ_0 was set to be 15° and L_1 be 7.5 mm to balance low Sc_peak and high shunt impedance. The other geometry parameters of the cross section were optimized to achieve large shunt impedance, as well as to keep high mechanical stability and facilitate cavity fabrication. For example, H_0 was chosen to be 38 mm to leave enough space for a cooling passage, and R_w was 0 mm to make the cavity split transversely easily. All the final cross-section parameters are listed in Table II except for $W_{\max}$, which would be finally determined when the whole cavity with modulation is calculated.

B. Design of pi-mode stabilizing loops (PISL)

According to the transmission-line model of the four-vane RFQ cavity and the perturbation theory for the eigenvalue problem [12,13], the local frequency error, caused by machining errors or vanes misalignment, provokes mode mixing between the operating quadrupole mode [as shown in Fig. 6(a)] and the neighboring dipole modes [Figs. 6(b) and 6(c)]. The mixing will break the field symmetry of the quadrupole mode and produce deviating forces in the transverse direction, causing emittance growth and beam loss. The perturbation theory also elaborates that the field asymmetry is in inverse proportion to the square difference of frequencies between the quadrupole mode and

TABLE II. Cross-section parameters of the HIAF RFQ.

Parameter	Value
θ_0 [deg]	15
θ_1 [deg]	22
θ_2 [deg]	3
L_1 [mm]	7.5
L_2 [mm]	11
H_0 [mm]	38
R_v [mm]	50
R_w [mm]	0
$W_{\max}$ [mm]	To be determined

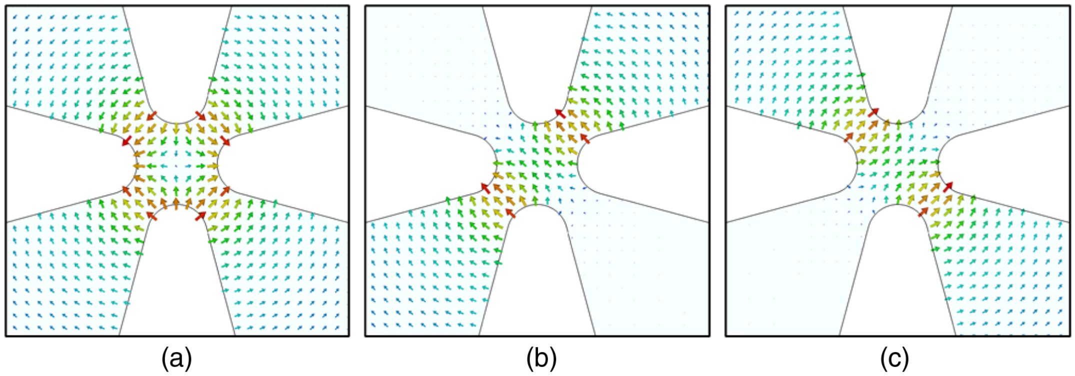

FIG. 6. Electric field patterns exist in an ideal four-vane RFQ (a: Quadrupole mode TE210; b: Dipole mode1 TE11n; c: Dipole mode2 TE11n).

the dipole modes. Although tuners can be used to correct the field asymmetry [14], the method will increase the tuning difficulties. Therefore, to mitigate the effects of the mode mixing on the beam, the mode separation between the quadrupole and the dipole modes is usually increased with some methods, such as vane coupling rings (VCRs) [15], dipole-mode stabilizer (DSR) [16], pi-mode stabilizing loops (PISL, as shown in Fig. 2), and coupling windows [17]. Because the PISL rods can be easily water-cooled, which is beneficial to high duty factor and cw operations, and also due to the extensive and successful experiences of employing PISL at IMP [14,18,19], the PISL method was adopted for the HIAF RFQ.

A universal criterion of acceptable frequency differences between the quadrupole mode and the dipole modes is in lack, even Ref. [7], in which PISL was first proposed, did not give what frequency difference was suitable. Therefore, we used the quadrupole field asymmetry as the criterion to design the PISL of the HIAF RFQ. The field asymmetry was required to be less than 1% by the HIAF RFQ beam dynamics, which aimed at reducing emittance growth and beam loss. In the simulation, it was assumed to be caused by vanes misalignment of ± 0.05 mm. Figure 7 shows one case of vanes misalignment, which generates the maximum field asymmetry with the mentioned alignment errors. In reality, the alignment error of the vanes is better than ± 0.03 mm with the state of the art of the RFQ fabrication technique based on the several RFQs built at IMP. Because the impacts of machining error were to be included, the alignment error was set to be ± 0.05 mm, putting a stricter demand on the PISL design.

In the PISL design, the field asymmetry was defined as the following formulas:

$$U_{d1} = \frac{0.5 \times (E_{Q1} - E_{Q3})}{E_{\mathrm{ave}}}$$

$$U_{d2} = \frac{0.5 \times (E_{Q2} - E_{Q4})}{E_{\mathrm{ave}}}$$

where U_{d1} and U_{d2} were the field asymmetries caused by the two kinds of dipole modes, respectively; E_{Q1}, E_{Q2}, E_{Q3} and E_{Q4} were the fields in the four quadrants of the four-vane RFQ, and $E_{\mathrm{ave}} = (E_{Q1} + E_{Q2} + E_{Q3} + E_{Q4})/4$. Values of U_{d1} and U_{d2} were sometimes different for the same misalignment case, but only the larger one was used.

The PISL design included the optimization of the period (Rod_P), distance (Rod_D), rods radius (R_rod), and the radius of the holes (R_RodHole) that the rods passed through, which are illustrated in Fig. 8. The relationship between the field asymmetry and the PISL geometry parameters is presented in Fig. 9. The quadruple mode frequency was kept at 81.25 MHz during the optimization by varying the transverse dimension $W_{\max}$.

Figure 9 shows that the field asymmetry (U_{d1} and U_{d2}) is reduced with decreased PISL rods period (Rod_P), rods distance (Rod_D), holes radius (R_RodHole), and increased rods radius (R_rod). Whereas, the frequency difference (F_D) changes in the opposite tendency, which

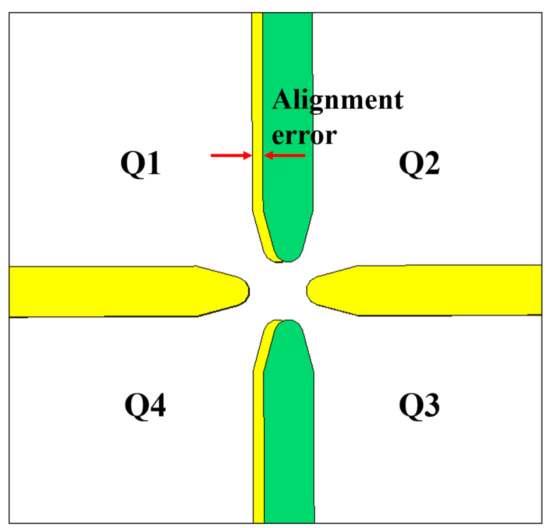

FIG. 7. Diagram of alignment error of four-vane RFQ vanes (yellow: ideal position of vanes, perfect symmetry; green: shifted position of vanes. Q1: first quadrant; and so on.).

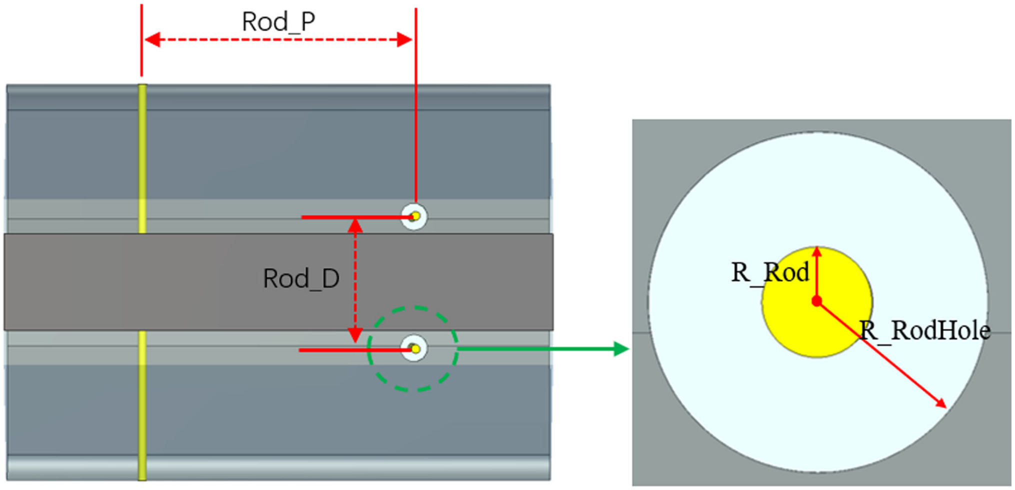

FIG. 8. Geometry of the PISL.

conforms with the perturbation theory. According to the operation mechanism of PISL [7], decreased rods period results in shortened magnetic field path and reduced inductance of dipole modes, thus raising the dipole mode frequencies; similarly, decreased rods distance increases the amount of detoured magnetic fields, which reduces the inductance and raises the frequencies of the dipole modes; decreased holes radius and increased rods radius raise the

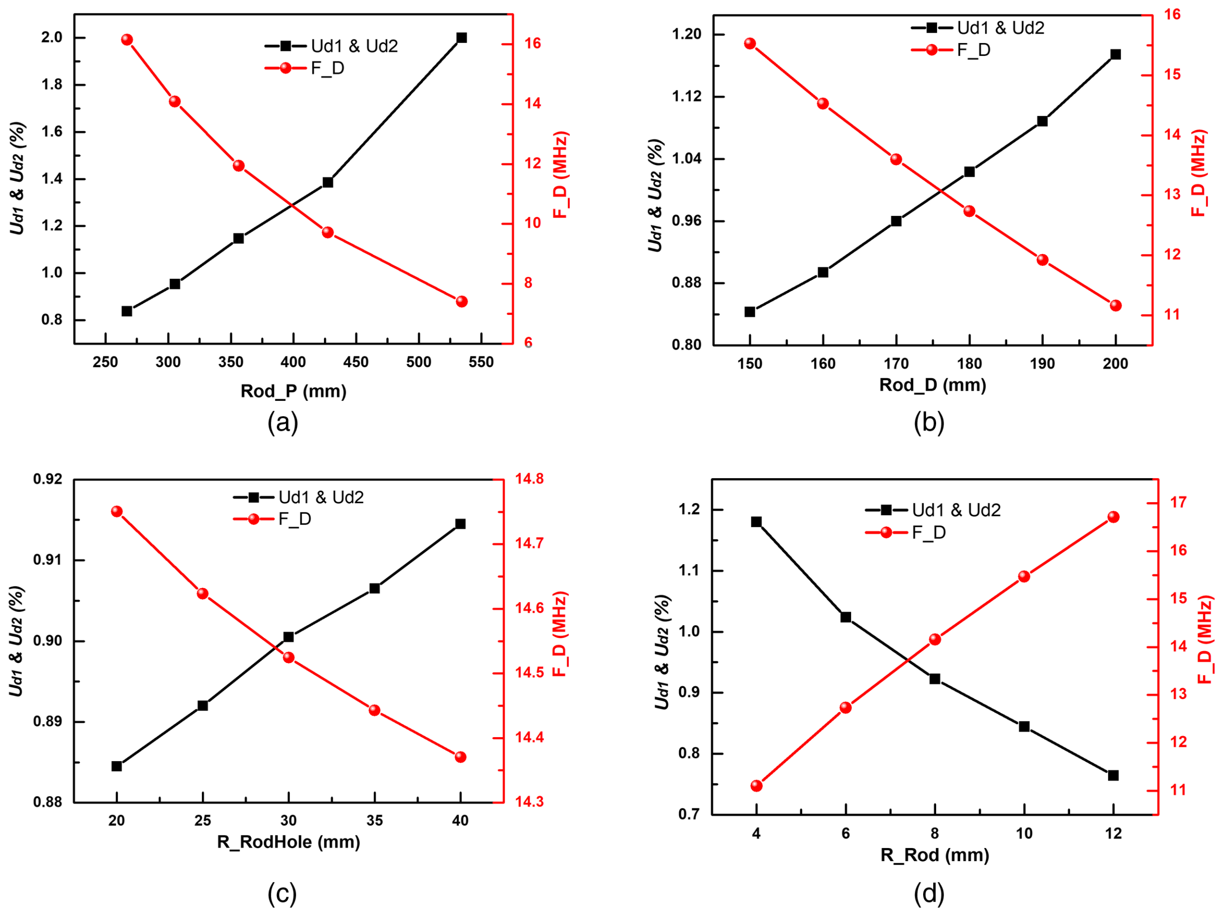

FIG. 9. Effects of PISL geometry parameters [(a) rods period Rod_P; (b) rods distance Rod_D; (c) holes radius R_RodHole; (d) rods radius R_rod] on field asymmetry (U_{d1} and U_{d2}) and frequency differences (F_D) between the operating quadrupole mode and neighboring dipole modes.

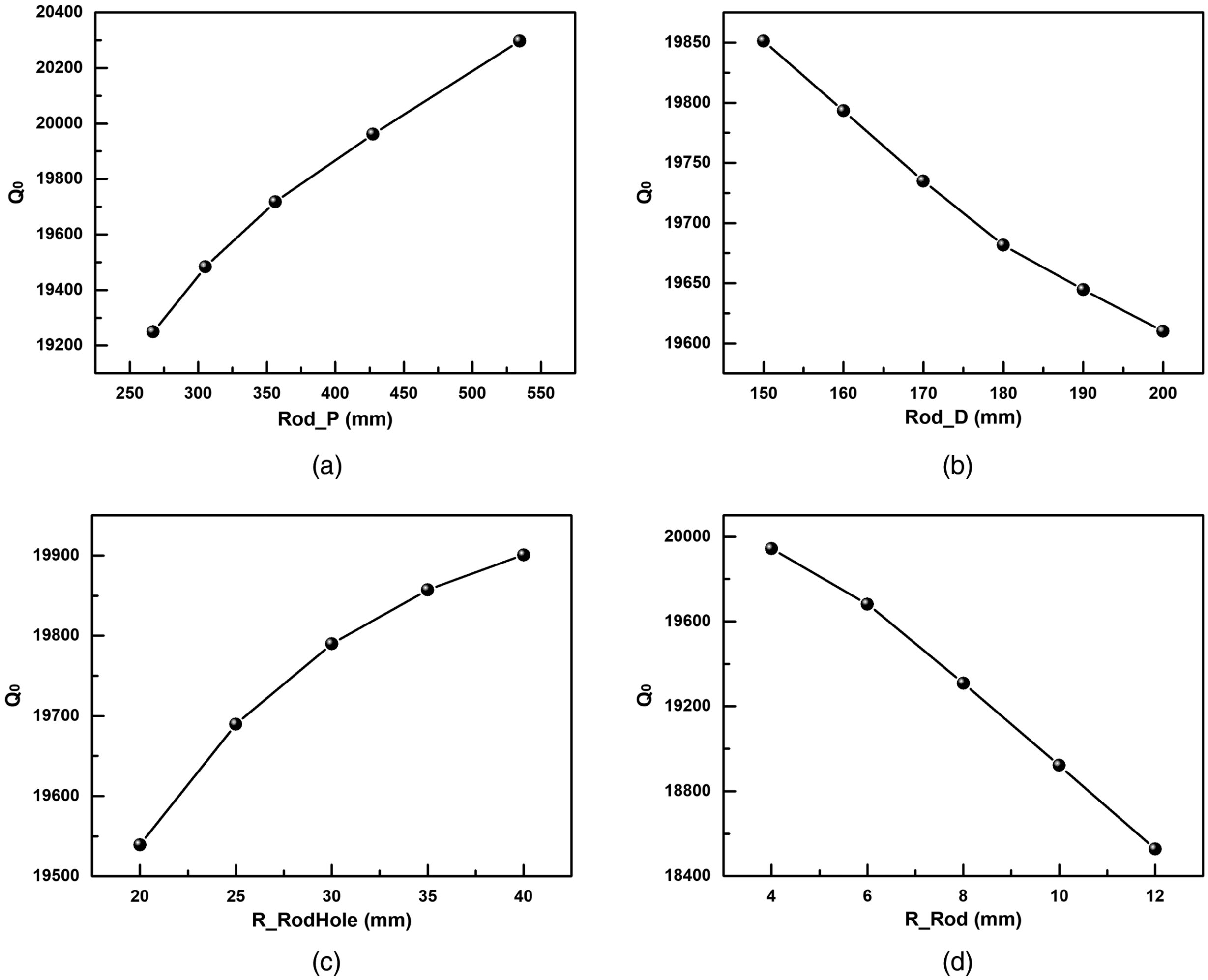

FIG. 10. Effects of PISL geometry [(a) rods period Rod_P; (b) rods distance Rod_D; (c) holes radius R_RodHole; (d) rods radius R_rod] on cavity quality factor Q_0.

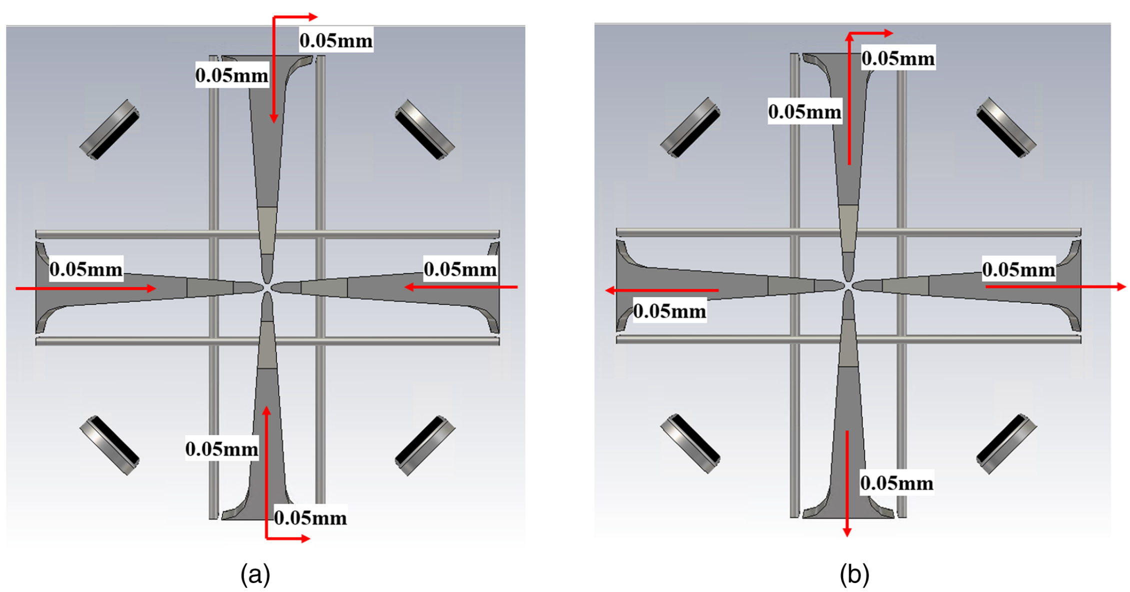

FIG. 11. Two cases of vanes misalignment: (a) Vanes were moving inward; (b) Vanes were moving outward. Arrows denoted the vanes moving directions.

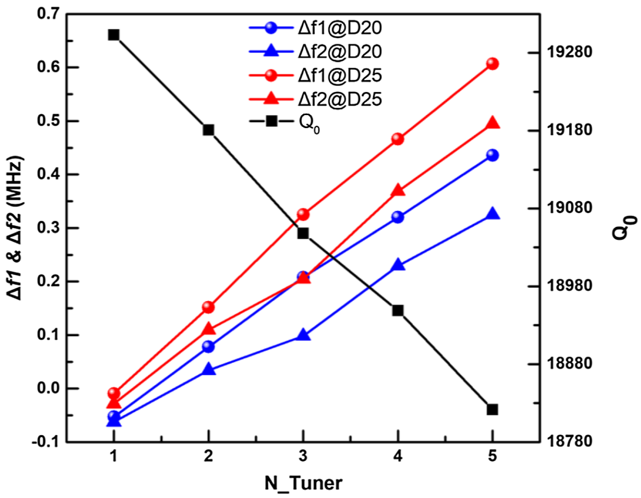

FIG. 12. Frequency tuning capability of tuners.

capacitance of the quadrupole mode, lowering the quadrupole frequency. Consequently, the frequency difference is expanded and the field asymmetry is decreased.

Meanwhile, the cavity quality factor Q_0 is affected by the PISL geometry, and Fig. 10 shows the effects. Q_0 decreases with decreased rods period, holes radius, and increased rods radius. Decreased rods distance results in increased Q_0; however, it is limited by the position of the cooling passage closest to the beam axis. Rod_P was finally set to be 316.66 mm which was the mean interval when there were 27 rod pairs in the HIAF RFQ, Rod_D, R_rod, and R_RodHole were chosen to be 170, 6, and 25 mm, respectively, and the final field asymmetry was 0.87%.

C. Tuner design

Tuners are utilized to tune cavity frequency, adjust longitudinal field flatness, and sometimes correct field asymmetry [14]. Since the field asymmetry is already better than 1% with PISL for the HIAF RFQ, tuners will only be employed to adjust field flatness and tune frequency. The desired field flatness can always be achieved by tuners with suitable quantity, size, and insertion depth. Therefore, the main goal of the HIAF RFQ tuner design was to compensate for the frequency error induced by machining and alignment errors. In the simulation, the frequency error was brought about by vanes misalignment as in the cases shown in Fig. 11. As mentioned in the PISL design, the real alignment error of the vanes is better than ± 0.03 mm, we adopted the error of ± 0.05 mm to include the influence of the machining error as well.

In Fig. 11(a), the four vanes were moved inward relative to the nominal position, resulting in a frequency decrease; and in Fig. 11(b), the vanes were moved outward, leading to a frequency increase. The absolute frequency changes were defined as Δf_{d} (frequency decrease) and Δf_{i} (frequency increase), respectively. Figure 12 shows the

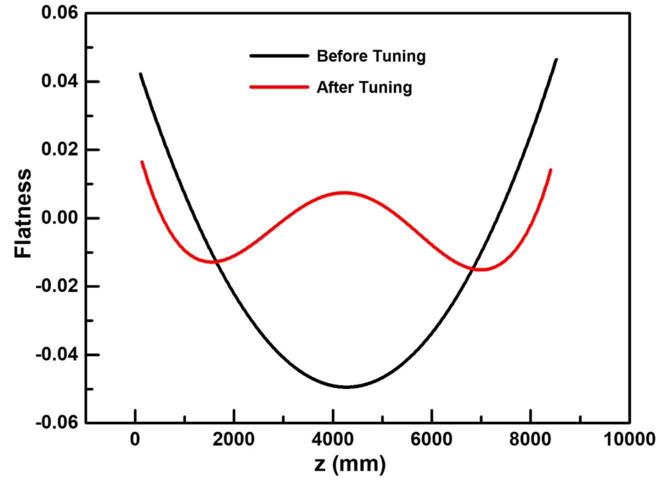

FIG. 13. Field flatness before and after tuning.

frequency tuning capability of tuners with a radius of 50 mm, where N_Tuner represents the number of tuners per meter in one quadrant, D20 and D25 mean the initial tuner's depth in the cavity of 20 mm and 25 mm, $\Delta f1 = \Delta f_{Ti} - \Delta f_d$ and $\Delta f2 = \Delta f_{Td} - \Delta f_i$. Δf_{Ti} is the frequency increment when tuners depth is 2 times the initial depth, Δf_{Td} is the absolute value of frequency decrement when tuners depth becomes 0 mm. The condition of $\Delta f1 > 0$ and $\Delta f2 > 0$ implies that the tuners have the ability to correct frequency error arising from vanes misalignment. Figure 12 indicates $\Delta f1 > 0$ and $\Delta f2 > 0$ when the number of tuners per meter ≥ 2, and $\Delta f1$ and $\Delta f2$ increase with the raising number of tuners. It can also be seen from Fig. 12 that D25 owns a greater tuning capability than D20 and the cavity quality factor Q_0 is decreasing when N_Tuner increases. By balancing the tuning capability against Q_0, the number of tuners per meter and the initial tuner's depth were finally set to be 3 and 25 mm, respectively.

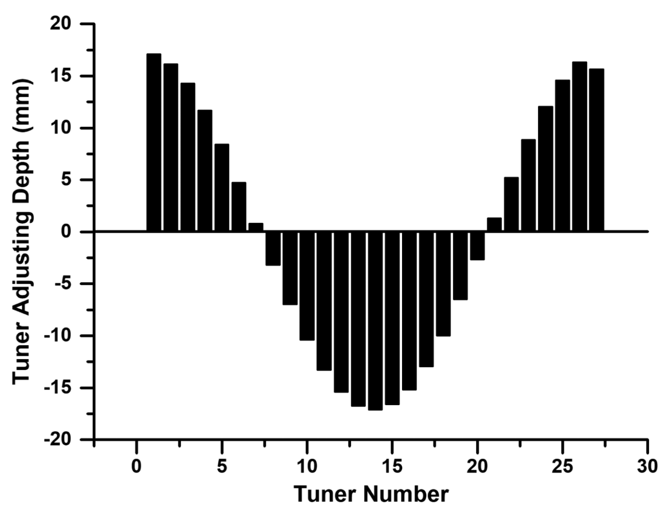

FIG. 14. Adjusting depth of the HIAF RFQ tuners to achieve the field flatness of $\pm 2\%$ from $\pm 5\%$.

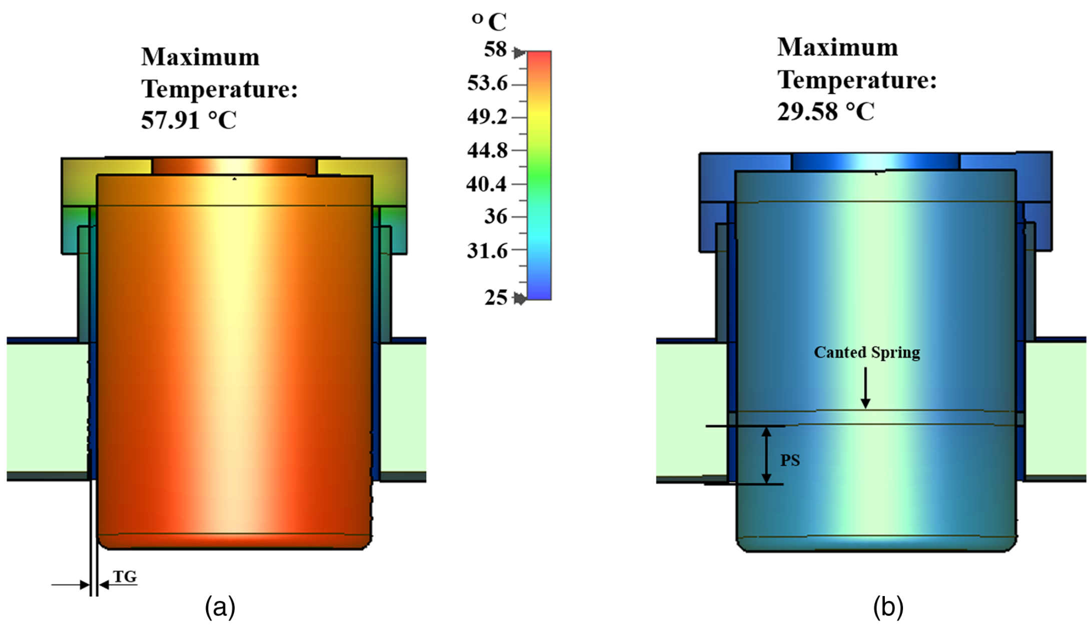

FIG. 15. Tuner installation (a): no rf sealing; (b): with rf sealing.

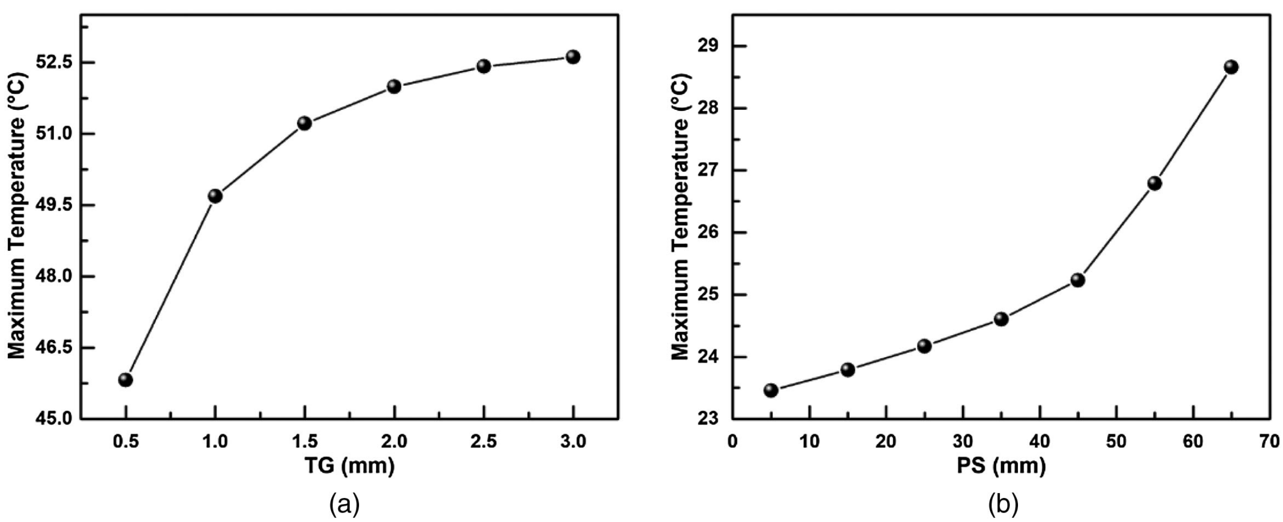

FIG. 16. (a): Relationship between tuner gap (TG) and maximum tuner temperature when no rf sealing; (b): Relationship between rf sealing position (PS) and maximum tuner temperature.

The field flatness before and after tuning with the optimized tuner quantity, size, and initial depth is displayed in Fig. 13. In the simulation, the field flatness before tuning was set at ± 0.05 when the tuners were at their initial depth, which represents the worst flatness of a real RFQ cavity before tuning based on the existing fabrication technique. Figure 14 presents the adjusting depth of the tuners along the RFQ, which can realize the required field flatness of ± 0.02 shown in Fig. 13. In Fig. 14, values below zero imply that tuners are pulled out from the initial depth, and values above zero imply that tuners are pushed in. Figure 14 demonstrates that the maximum pull-out depth is about 17 mm which is less than the initial depth. It can be concluded that the designed tuners can meet the adjusting requirement of the longitudinal field flatness.

The temperature distribution of tuners depends highly on the installation of the rf sealing (e.g., canted spring). Figure 15 displays two tuner installation methods (with and without rf sealing) and the corresponding temperature distributions. It can be seen that the rf sealing can lower the maximum temperature by nearly half. Furthermore, Fig. 16(a) shows a narrow tuner gap (TG in Fig. 15) brings about a low maximum temperature when there is no rf sealing; Fig. 16(b) exhibits a short distance of the rf sealing to

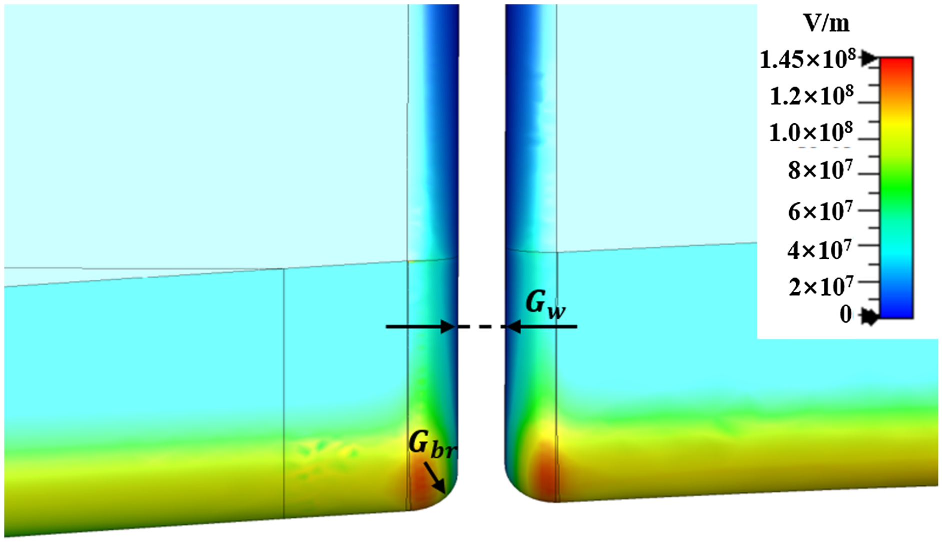

FIG. 17. Geometry of the gap between vane tips (G_w: gap width; G_{br}: radius of blend edge).

the cavity's inner surface (PS in Fig. 15) results in a low peak temperature too. It is believed that the heat in the tuner is conducted better when the tuner gap is narrow, and the heat flow on the tuner is low when the rf sealing is close to the cavity's inner surface. Based on the analysis, rf sealing is necessary to be installed for the HIAF RFQ tuners.

D. Peak surface electric field and vanes segmentation

An RFQ is often fabricated in segments when the cavity length exceeds the machining range of a machine tool, and then the segments are joined together. The peak electric field usually occurs in the gap between the vane tips at the segment interfaces [11,20–22]. To reduce the possibility of rf electric breakdown caused by the high electric field in the gap, the gap geometry was optimized. Figure 17 depicts the gap geometry, where G_w denotes the gap width and G_{br} means the radius of the blend edge. The influences of G_w and G_{br} on the peak surface electric field, expressed as KP, are illustrated in Fig. 18. For the HIAF RFQ, the field is 10.536 MV/m when KP is 1. Figure 18 suggests the peak surface electric field is greatly affected by the gap width when the blend edge is sharp (e.g., $G_{br} < 0.2$ mm). However, once G_{br} increases, the influence of the gap width disappears and the peak surface electric field decreases slowly. Considering the effect of the gap on the beam transport, 0.5 and 1.0 mm were chosen for G_w and G_{br}, respectively.

The effect of the gap position (P_Gap) in a unit cell on the peak surface electric field is illustrated in Fig. 19. The length of the unit cell in Fig. 19 is 76 mm, and the position of 38 mm in the center of the unit cell. Figure 19 indicates the peak surface electric field reaches a minimum value when the gap is at the center of the unit cell, which agrees

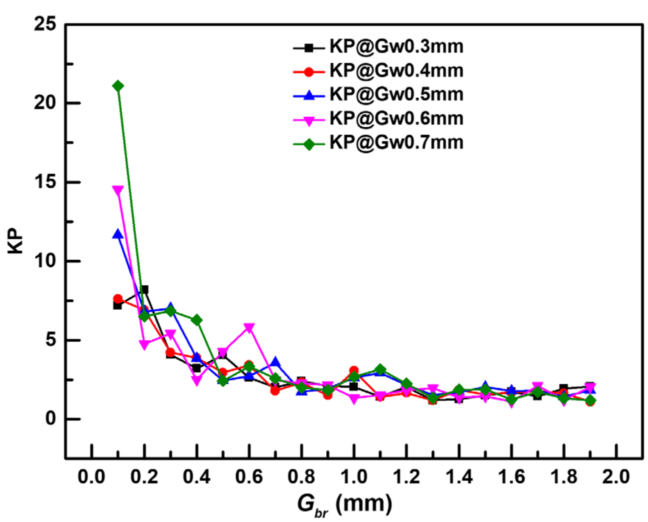

FIG. 18. Influence of G_w and radius of blend edge G_{br} on peak surface electric field.

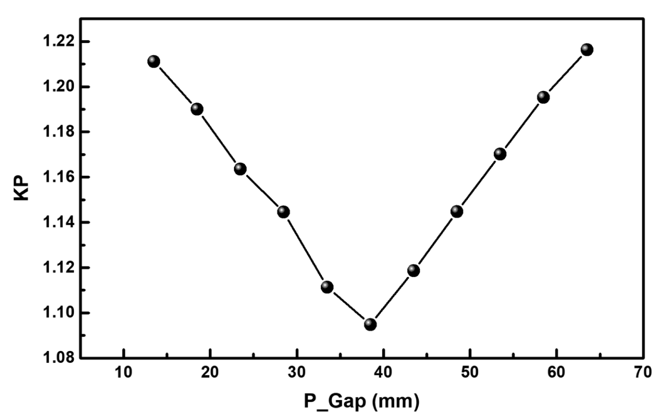

FIG. 19. Relationship between the peak surface electric field in the vane tips gap and the gap position (P_Gap) in a unit cell (cell length = 76 mm).

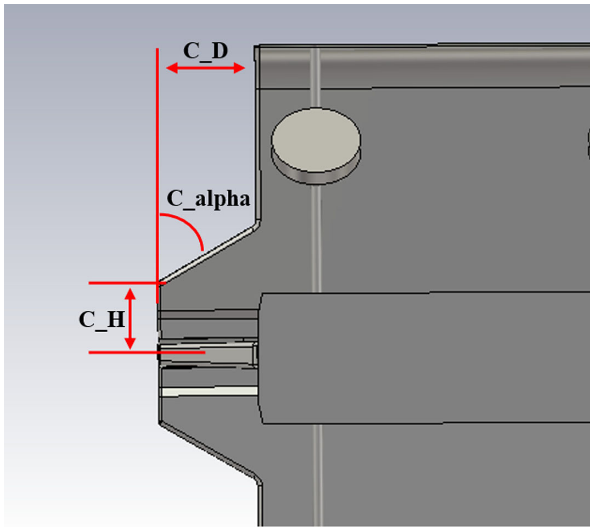

FIG. 20. Sketch map of the undercut.

with the result in Ref. [11] and provides a benchmark for the RFQ segments division. The effect of vanes misalignment between adjacent segments on the peak surface electric field was investigated too, and the result demonstrates the influences are negligible when G_{br} is 1 mm.

E. Undercut design

Gaps exist between the vanes and the end walls at the two ends of the four-vane RFQ cavity, allowing the magnetic fields turning direction reversely between adjacent quadrants [23]. Due to the lower capacitances and inductances, the frequencies in the gaps are higher than the frequencies among the vanes, which results in a field dropping at the two ends. Tuners cannot raise the field at the ends due to the far distance. Undercut (as shown in Fig. 20) was proposed to solve the problem, which can lower the frequency of the quadrupole mode in the gaps by introducing extra inductances [24]. Figure 21 displays the field flatness with and without undercut. The undercut design is mainly restricted by the thermal and mechanical requirements [25]. Through optimization, the final undercuts parameters of the HIAF RFQ were obtained and shown in Table III. The undercut depths (C_D in Fig. 20) at the two ends are different, the reason is that the modulations were included when designing the undercuts, and the local frequencies at the ends were varied with modulations [26].

TABLE III. Undercuts parameters of the HIAF RFQ.

Parameter	C_H [mm]	C_alpha [mm]	C_D [mm]
Input end	80	60	116
Output end	80	60	111

TABLE IV. Main rf parameters of the HIAF RFQ.

Parameter	Value
W_{max} [mm]	342.5
Quadrupole frequency [MHz]	81.2502
Dipole frequency [MHz]	95.8302
Power [kW]	98.74
Q_0	18362.9
Peak surface electric field [MV/m]	20.883
Field flatness	within ± 0.01

F. rf Simulation of the whole cavity

The transverse dimension W_{max} of the HIAF RFQ was finally determined when PISL, tuners, and undercut were fixed. All the rf parameters of the cavity were obtained by simulating the whole cavity and summarized in Table IV. The final transverse dimension is 342.5 mm and the frequency difference between the quadrupole mode and closest dipole mode is 14.58 MHz. The peak surface electric field is 20.883 MV/m when the field flatness is within $\pm 1\%$, which is a little higher than the value given by the beam dynamics design, located in the middle of the 203rd unit cell where the eighth and ninth segments are

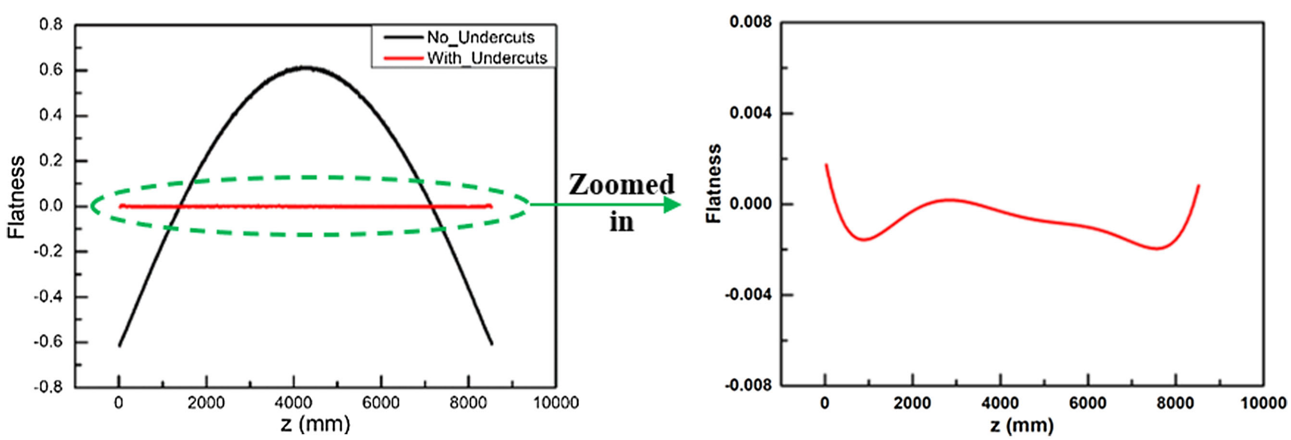

FIG. 21. Field flatness with and without undercuts.

connected. It should be noted that the value and location of the peak surface electric field are affected by the field flatness, therefore, it is necessary to mention the field flatness when talking about the peak surface electric field of an RFQ.

IV. MULTIPHYSICS ANALYSIS OF THE HIAF RFQ CAVITY

Multiphysics analysis of the RFQ cavity includes the design of cooling channels and the analysis of the wall thickness effects on the cavity mechanical stress and deformation, and it was performed with ANSYS Workbench [27]. In the analysis, rf calculation of the cavity was first carried out; then, the thermal calculation was conducted with thermal losses from rf calculation. Next, the structural calculation was performed with the temperature distribution from the thermal analysis. Finally, the rf calculation was done again with the deformed structure derived from the structural calculation.

A. Design of cooling channels

For a cw RFQ, cavity cooling plays an essential role in the long-term stable operation. The basic function is taking heat away to maintain the cavity's resonant frequency fixed and to further make the operating frequency close to the design frequency as much as possible [28]. In addition, for the HIAF RFQ, zero frequency change is required, when the input rf power varies for the acceleration of ions with different charge-to-mass ratios, to avoid changing the cooling water temperature frequently. To meet the requirements, the layout of the cooling channels was designed to realize zero Δf when the input power was different, where $\Delta f = f_{\text{full power}} - f_{\text{no power}}$, $f_{\text{full power}}$ and $f_{\text{no power}}$ are the cavity frequency with full rf power and no power, respectively.

Based on our calculation, running with full power, the water temperature increase in the cooling channels of one segment was approximately 1 °C. The cavity frequency variation induced by the increased temperature was only about 2 kHz, whose effect on the field was tiny. Therefore, the water temperature increase was not considered during the analysis.

The layout of the cooling channels of the HIAF RFQ is displayed in Fig. 22. It has 12 channels in the 4 vanes and 8 channels in the walls. The diameters of the cooling channels are 12 mm except for channel V1, which is 10 mm because of the narrow local vane width. The position of V1 is 50 mm from the beam axis, which is determined by the position of rod holes. The positions of W1 and W2 are 90 mm from the tuner center and 25 mm from the cavity's inner surface, which is determined by the positions of sealing grooves and welding seams. The positions of V2 (P_V2) and V3 (P_V3) are to be decided with the goal of realizing zero Δf. In view of the high ambient temperature

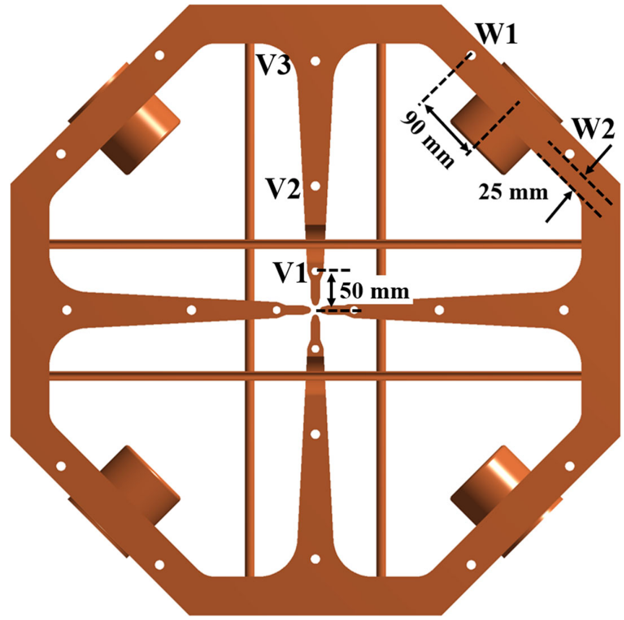

FIG. 22. Layout of the HIAF RFQ cooling channels.

in southern China, the inlet water temperature and ambient temperature were set at 25 °C when performing the multiphysics analysis. The water velocity was decided to be 1.5 m/s, based on the actual running situation of the water system at IMP.

Figure 23 shows the position influences of channels V2 and V3 on Δf, which illustrates that $\Delta f = 0$ can be achieved by arranging the positions of V2 and V3 reasonably. However, there is an upper limit for the V3 position; for example, there is no V2 position to make Δf zero when V3 position is 315 mm. The positions of channels V2 and V3 were finally determined to bring the operating frequency of the cavity close to the design frequency as much as possible. In real cases, these positions are 164.5 and 314.3 mm away from the beam axis, respectively.

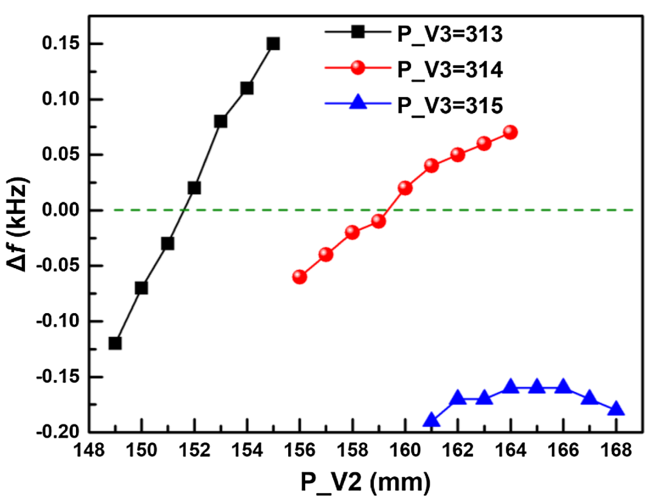

FIG. 23. Position influences of channels V2 and V3 on Δf.

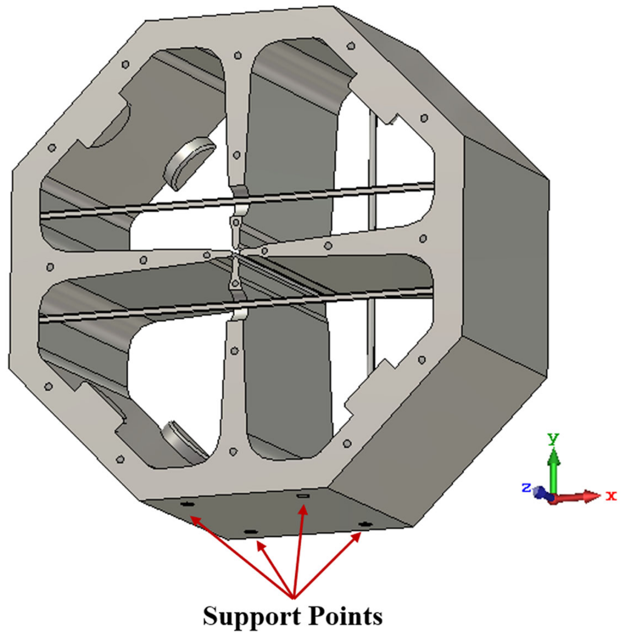

FIG. 24. RFQ module with a length of one PISL period.

The cavity frequency sensitivity to water temperatures was investigated when the layout of the cooling channels was determined. Results show the sensitivity is 18.49 kHz/°C and −20.51 kHz/°C to the wall and vane water, respectively, and the cavity frequency decreases by 2.02 kHz when both the wall and vane water temperature increase by 1 °C.

B. Effects of wall thickness on the cavity mechanical stress and deformation

The mechanical stress and deformation of the RFQ cavity are greatly affected by the wall thickness. To ensure the stable and reliable operation of the HIAF RFQ, the effects of the wall thickness have been investigated. One module with a length of one PISL period was used to perform the investigation, and it was assumed to be supported by four points, as shown in Fig. 24. The earth's gravity, vacuum, and rf power were all included in the analysis.

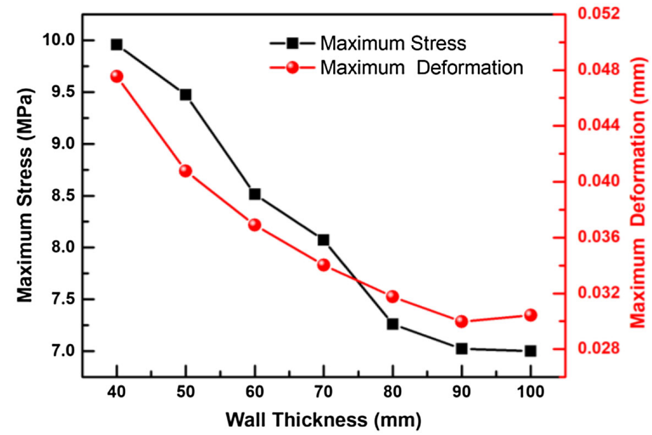

FIG. 26. Influence of wall thickness on the maximum stress and deformation of RFQ cavity.

Figure 25 displays the distributions of the equivalent stress and deformation of the cavity, and Fig. 26 exhibits the effects of the wall thickness on the maximum stress and deformation. Both the maximum stress and deformation decrease when the wall thickness increases from 40 to 90 mm, and the stress is far below the yield strength of the annealed copper (about 70 MPa [29]). The deformation of the 100 mm thickness becomes a little larger than that of the 90 mm thickness. It was found the maximum deformation of the 100 mm thickness wall was located on the wall, as shown in Fig. 27. Whereas, the maximum deformation appeared on the horizontal PISL rods when the wall thickness was not larger than 90 mm (see Fig. 25). The investigation suggests that it is preferable to adopt a large wall thickness to obtain low stress and minor deformation

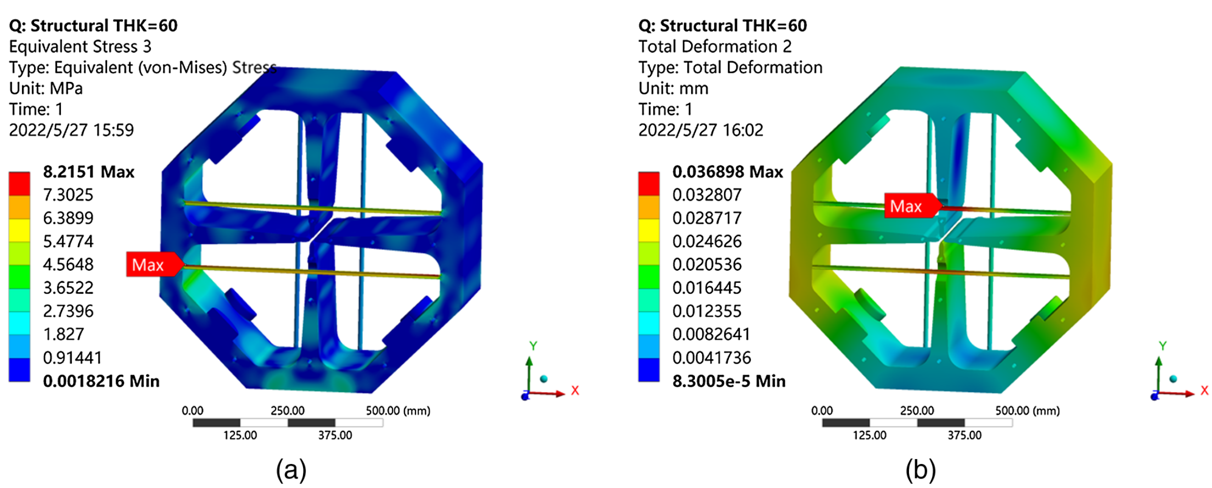

FIG. 25. Stress (a) and deformation (b) distributions of one HIAF RFQ cavity with a wall thickness of 60 mm.

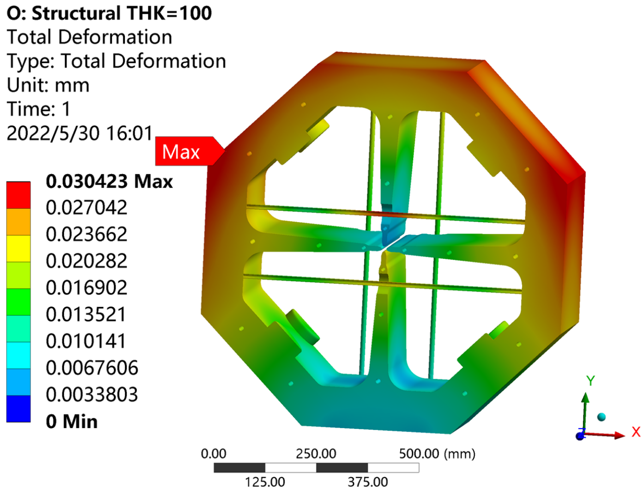

FIG. 27. Deformation distribution of RFQ cavity with a wall thickness of 100 mm.

of the cavity. Nevertheless, the final wall thickness of the HIAF RFQ was set at 70 mm to save copper, meanwhile, to keep low stress and minor deformation.

V. SUMMARY

A cw RFQ was designed for the injector linac of the HIAF project. To achieve high stability and reliability for the long-term operation, the rf design and multiphysics analysis of the cavity were carefully performed.

To minimize the rf breakdown rate in the RFQ cavity, the cross section was optimized to reduce the peak modified Poynting vector, and the gap between vane tips at the segment interfaces was optimized to lower the peak surface electric field. It was found that there existed an optimal θ_0 (breakout angle of the vane tip) that could produce a minimum peak modified Poynting vector. The final θ_0 was set at 15° (different from other RFQs at IMP with 10° θ_0) to avoid the impact on the cavity shunt impedance. It was observed that the electric field in the gap reached a minimum value when the gap was in the center of a unit cell, and a large radius of the blend edge of the gap produced a low electric field.

To reduce the emittance growth and beam loss caused by the field asymmetry of the quadrupole mode, the PISL was adopted to mitigate the effects of mode mixing between the operating quadrupole mode and the neighboring dipole modes. Research results demonstrate that decreased PISL rods period and rods distance and increased rod radius can improve field symmetry. Tuners were designed to regulate cavity frequency and adjust field flatness longitudinally. Simulation results indicate that tuners with a large total number, large radius, and great initial depth possess a high-frequency tuning and field flatness adjusting capability. The rf sealing between the tuners and cavity wall is indispensable in reducing the tuner's temperature.

A multiphysics analysis was carried out for the HIAF RFQ cavity. It was demonstrated that reasonably arranging the cooling channels could achieve zero frequency change with different rf power. The analysis also shows that a large wall thickness can make the cavity possess low stress and minor deformation.

The design of the HIAF RFQ, including rf design, multiphysics analysis, and mechanical design, has been completed. The construction of the cavity is scheduled to be finished by the end of 2022. A solid-state rf amplifier of 140 kW has been ordered for the RFQ; the first beam test is expected to conduct in March of 2023.

ACKNOWLEDGMENTS

This work is supported by High Intensity heavy-ion Accelerator Facility (HIAF) approved by the National Development and Reform Commission of China.

[1] L. J. Mao, J. C. Yang, D. Q. Gao *et al.*, Status of the HIAF accelerator facility in China, in *Proceedings of the 27th Russian particle accelerators conference, RuPAC2021, Alushta, Russia, 2021* (JACOW, Geneva, Switzerland, 2021).

[2] L. M. Young, L. J. Rybarcyk, J. D. Schneider *et al.*, High power operations of LEDA, in *Proceedings of the 20th International Linac Conference, LINAC-2000, Monterey, CA, 2000* (SLAC, Menlo Park, CA, 2000).

[3] E. Fagotti, L. Antoniazzi, L. Bellan *et al.*, Beam commissioning of the IFMIF EVEDA very high power RFQ, in, *Proceedings of the 9th International Particle Accelerator Conference, IPAC-2018, Vancouver, Canada, 2018* (JACoW, Geneva, Switzerland, 2018).

[4] H. Shi, H. F. Ouyang, S. C. Wang, N. C. Zhou, and G. Wu, rf tuning and beam commissioning of cw RFQ for China-ADS injector-I, Nucl. Sci. Tech. **29**, 142 (2018).

[5] T. P. Wangler, *RF Linear Accelerators* (Wiley-VCH Verlag GmbH & Co. KGaA, Weinheim, 2008), pp. 163–164.

[6] Lloyd Young, Tuning and stabilization of RFQs, in *Proceedings of the Linear Accelerator Conference, Albuquerque, NM, USA* (JACOW, Geneva, Switzerland, 1990).

[7] A. Ueno and Y. Yamazaki, New field stabilization method of a four-vane type RFQ, Nucl. Instrum. Methods Phys. Res., Sect. A **300**, 15 (1991).

[8] A. Grudiev, S. Calatroni, and W. Wuensch, New local field quantity describing the high gradient limit of accelerating structures, Phys. Rev. ST Accel. Beams **12**, 102001 (2009).

[9] S. Verdu-Andres, U. Amaldi, R. Bonomi *et al.*, High-gradient test of a 3 GHz single-cell cavity, in *Proceedings of the 25th International Linear Accelerator Conference, LINAC-2010, Tsukuba, Japan* (KEK, Tsukuba, Japan, 2010).

[10] S. Benedetti, A. Grudiev, and A. Latina, High gradient linac for proton therapy, Phys. Rev. Accel. Beams **20**, 040101 (2017).

[11] Hermann Pommerenke, Compact radio-frequency quadrupoles for industrial and medical applications, doctoral dissertation, 2020, 10.18453/rosdok_id00002956.

[12] T. P. Wangler, RF Linear Accelerators (Wiley-VCH Verlag GmbH & Co. KGaA, Weinheim, 2008), pp. 254–260.

[13] A. Palmieri, Preserving beam quality in long RFQs on the rf side: voltage stabilization and tuning, in *Proceedings of 54th ICFA Advanced Beam Dynamics Workshop on High-Intensity, High Brightness and High Power Hadron Beams, East-Lansing, MI, 2014* (JACoW, Geneva, Switzerland, 2014).

[14] W. Ma, L. Lu, T. Liu, L. B. Shi, L. P. Sun, C. X. Li, W. B. Wang, X. B. Xu, T. He, Y. He *et al.*, Frequency and fields tuning of a heavy ion radio-frequency quadrupole accelerator, Nucl. Instrum. Methods Phys. Res., Sect. A **901**, 180 (2018).

[15] H. R. Schneider and H. Lancaster, Improved field stability in RFQ structures with vane coupling rings, IEEE Trans. Nucl. Sci. **30**, 3007 (1983).

[16] F. Grespan, A. Pisent, and A. Palmieri, Dipole stabilizers for a four-vane high current RFQ: Theoretical analysis and experimental results on a real-scale model, Nucl. Instrum. Methods Phys. Res., Sect. A **582**, 303 (2007).

[17] B. Mustapha, A. A. Kolomiets, and P. N. Ostroumov, Full three-dimensional approach to the design and simulation of a radio-frequency quadrupole[J], Rev. Mod. Phys. **16**, 120101 (2013).

[18] Z. L. Zhang, Y. He, B. Zhang, D. R. Li, A. M. Shi, G. Pan, X. N. Du, and L. P. Sun, Study of influence of radial matcher section end shape on RFQ cavity frequency, Chin. Phys. C **38**, 077007 (2014).

[19] C. X. Li, Y. He, X. B. Xu, Z. L. Zhang, F. F. Wang, W. P. Dou, Z. J. Wang, and T. S. Wang, rf structure design of the China Material Irradiation Facility RFQ, Nuclear Instrum. Methods Phys. Res., Sect. A **869**, 38 (2017).

[20] M. DI Giacomo, R. Ferdinand, H. Franberg *et al.*, rf commissioning of the SPIRAL2 RFQ in CW mode and beyond nominal field, in *Proceedings of the 10th International Particle Accelerator Conference, IPAC-2019, Melbourne, Australia, 2019* (JACoW, Geneva, Switzerland, 2019).

[21] M. Comunian, Beam dynamics issues in high-current RFQs, in *Proceedings of the "High Intensity RFQ meets Reality" Workshop, Heidelberg, 2019* (GSI, Heidelberg, Germany, 2019).

[22] I. Bustinduy and J. L. Muñoz, Technical Design Report No. ESSB-Rep-2015-10, 2015 [ISBN-13: 978-84-616-5445-1].

[23] Richard H. Stokes and Thomas P. Wangler, Radiofrequency quadrupole accelerators and their applications, Annu. Rev. Nucl. Part. Sci. **38**, 97 (1988).

[24] L. M. Young, Segmented resonantly coupled radio-frequency quadrupole (RFQ), in *Proceedings of the 15th Particle Accelerator Conference, PAC-1993, Washington, DC, 1993* (IEEE, New York, 1993).

[25] V. V. Paramonov, One aspect of thermal stability for 4-vane RFQ operation with high heat loading, in *Proceedings of RuPAC 2010, Protvino, Russia* (JACOW, Geneva, Switzerland, 2010).

[26] Chenxing Li, Design and test of the China material irradiation facility RFQ, doctoral dissertation, 2018, https://ir.lzu.edu.cn/handle/262010/211816.

[27] ANSYS, http://www.ansys.com.

[28] Q. Z. Xing, J. Zeng, S. X. Zheng, J. Li, X. L. Guan, C. X. Tang, and X. W. Wang, rf-induced frequency-shift resistant design of the resonant cavity of the radio frequency quadrupole with the high average-power operation, Nucl. Instrum. Methods Phys. Res., Sect. A **904**, 117 (2018).

[29] Brookhaven National Laboratory, Selected Cryogenic Data Notebook (1980), Vol. **1**, https://www.osti.gov/biblio/7031380-brookhaven-national-laboratory-selected-cryogenic-data-notebook-volume-sections#.